Active Surface Structure of SnO2 Catalysts for CO2 Reduction Revealed by Ab Initio Simulations

THE JOURNAL OF PHYSICAL CHEMISTRY C
A JOURNAL OF THE AMERICAN CHEMICAL SOCIETY

pubs.acs.org/JPCC

Article

Active Surface Structure of SnO_2 Catalysts for CO_2 Reduction Revealed by Ab Initio Simulations

Clara Salvini,* Michele Re Fiorentin,* Francesca Risplendi, Federico Raffone, and Giancarlo Cicero

Cite This: *J. Phys. Chem. C* 2022, 126, 14441−14447

Read Online

ACCESS | Metrics & More | Article Recommendations | Supporting Information

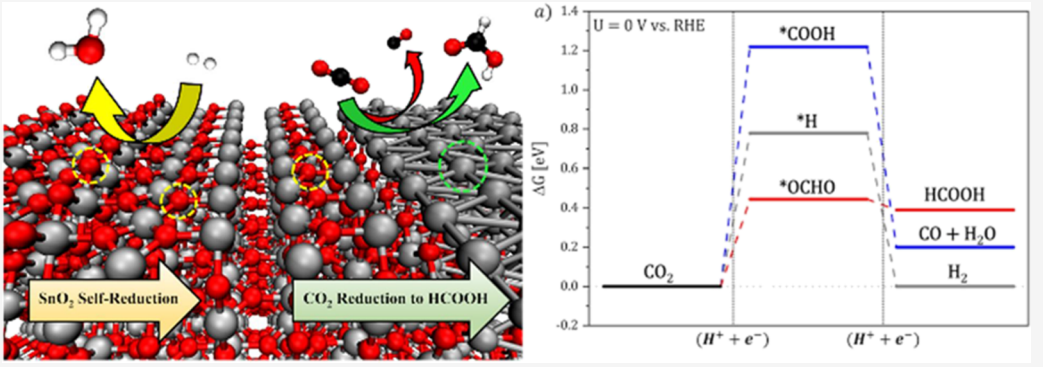

ABSTRACT: Tin oxide (SnO_2) is an efficient catalyst for the CO_2 reduction reaction (CO_2RR) to formic acid; however, the understanding of the SnO_2 surface structure under working electrocatalytic conditions and the nature of catalytically active sites is a current matter of debate. Here, we employ *ab initio* density functional theory calculations to investigate how the selectivity and reactivity of SnO_2 surfaces toward the CO_2RR change at varying surface stoichiometry (i.e., reduction degree). Our results show that SnO_2(110) surfaces are not catalytically active for the CO_2RR or hydrogen evolution reaction, but rather they reduce under an applied external bias, originating surface structures exposing few metal tin layers, which are responsible for formic acid selectivity.

INTRODUCTION

In the last few decades, due to the progressive industrial development and the improvement of the living standard, the anthropogenic emission of carbon dioxide (CO_2), one of the gases mainly responsible for greenhouse effects, has steadily increased to a level that has raised the worries of the international community because it may lead to catastrophic environmental impact.[1] This problematic scenario has received great attention by the scientific communities, and new technologies for CO_2 capture and reuse are currently at an explorative research level.[2]

Among others, electrochemical CO_2 reduction is a promising strategy toward carbon recycling and atmospheric CO_2 content mitigation.[3] This conversion process consists in the transformation of CO_2 into value-added compounds by application of an external voltage to an electrolyzer: the CO_2 dissolved in the electrolytic solution adsorbs and gets reduced at the cathode. This approach has several advantages, such as the possible coupling to renewable energy sources to power the system, and it is in principle suited for large-scale sustainable implementation.[4,5] However, the accomplishment of CO_2 electroreduction is difficult to be achieved owing to the high thermodynamic stability of the carbon dioxide molecule. Moreover, the conversion involves slow kinetics, because of high energy reaction barriers, and poor selectivity due to undesired side reactions. The employment of highly stable, robust electrocatalysts deposited on the cathode is fundamental to solve the efficiency and selectivity issues in the electrochemical CO_2 reduction reaction (CO_2RR) and to reduce the reaction overpotential.[6,7]

Among the possible high-value-added reduction compounds, formic acid (HCOOH) is one of the most interesting because it may serve as a raw material for molecular hydrogen or carbon monoxide (CO) production via decarboxylation and decarbonylation, respectively.[8−11] Nanostructured noble metals, such as gold, silver, and palladium, are excellent catalysts toward reaction products with a single carbon atom (C1), but they are too expensive to be extensively used in industrial processes.[12−16] To decrease the cost, attention has been directed to non-noble metal catalysts, which also exhibit promising catalytic performance.[17−22] Particularly, metal tin is a low-cost element abundant in the Earth's crust, whose

Received: April 14, 2022
Revised: July 29, 2022
Published: August 22, 2022

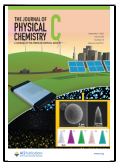

applications as an electrocatalyst have recently grown because of its high activity as well as its eco-friendly properties.[23,24] Sn is reported to be selective toward HCOOH production because its high oxygen affinity induces a bidentate *OCHO intermediate, required for formic acid evolution.[25−30] In the case of Sn, an oxide layer rapidly forms at the surface of the metal exposed to air. Consequently, a common practice consists of using tin dioxide (SnO_2) covered electrodes because SnO_2 samples typically present a higher specific area and roughness, and they are supposed to get reduced to metallic tin at working electrocatalytic potentials.[32−36]

Notwithstanding the acknowledged efficiency of SnO_2 electrocatalysts, a current matter of debate in the literature regards the nature of the electrocatalyst active surface, resulting in conflicting interpretations. According to the Sn−O Pourbaix diagram,[31] under electrocatalytic CO_2 reduction conditions toward formate ($HCOO^-$) production, that is, at low applied potential ($U < -0.4$ V) and pH > 4, the thermodynamically stable phase is metallic tin (Sn^0).[32] Thus, the SnO_2 particles deposited on the electrode should be completely reduced under working electrode conditions. On the other hand, several studies have reported that tin oxide phases are still present at the cathode surface when CO_2 gets reduced. As an example, Lee and co-workers[33] performed CO_2 reduction on SnO_2 at different alkaline pH values and found that at high pH values (10.2 and 11.72) the catalysts' X-ray diffraction (XRD) spectra reveal only tin oxide phases and that, under these conditions, a high selectivity toward formic acid is observed. On the contrary, under mild basic conditions (pH = 8.42) the catalyst is partially reduced to metallic Sn and, correspondingly, a decrease of formic acid faradaic efficiency and an increase in hydrogen production are reported.[33] In contrast, Gao et al.[34] stated that a moderate degree of SnO_2 reduction is fundamental for the reduction of CO_2 to formic acid. In particular, it was found that the loss of oxygen species from the oxide surface leads to a rich oxygen vacancy system which is believed to be responsible for the selective reduction of CO_2 to formic acid.

To gain a deeper insight into the structure and reactivity of the SnO_2 catalytic active surface, few research groups performed operando Raman spectroscopic characterization. Both Dutta and collaborators[35] and Kuzume et al.[36] reported that the highest selectivity toward formate occurred at potentials where SnO_2 should be completely reduced according to Pourbaix analysis, yet their measurements revealed that in this potential range (approximately between −0.5 and −1.1 vs Ag|AgCl at different pH values) SnO_2 samples appear to be only partially reduced. Hence, they suggest that SnO_2 reduction is kinetically hindered. Based on this evidence, the authors concluded that both Sn^0 and Sn^{II} are present during the CO_2RR, although it is not clear which species plays the major catalytic role during the reaction. Moreover, the authors found that at very negative potentials, all SnO_2 is reduced to metallic Sn and HCOOH production drops, in favor of hydrogen production.

In summary, despite the large research effort of the last few years, the understanding of the SnO_2 surface structure under working electrocatalytic conditions and the nature of catalytically active sites for CO_2 reduction have not been identified yet. Reaction pathways and mechanistic studies of the CO_2RR on SnO_2 electrocatalysts have been mainly performed by theoretical calculations, investigating the effect of a moderate number of oxygen vacancies,[37] the presence of surface hydroxyls[38] and the use of doping agents,[32,39,40] but a uniform computational model about the involved surface termination at experimental conditions does not exist yet.

In this paper, we employ *ab initio* density functional theory (DFT) calculations to investigate how the selectivity and reactivity of SnO_2 surfaces toward the CO_2RR change at varying degree of reduction. We compare the free energy profiles for the CO_2RR and the competing hydrogen evolution reaction (HER) and discuss the surface features responsible for HCOOH selectivity. Our results reveal that the stoichiometric SnO_2 surface is not catalytically active and spontaneously loses oxygen species at low applied potential. This spontaneous oxygen loss leads to tin-rich metallic surfaces, which become selective toward HCOOH products when at least a Sn bilayer is formed at the catalyst surface. When SnO_2 is completely reduced to metal, molecular hydrogen evolution becomes competitive.

THEORETICAL METHODS

Our theoretical predictions are based on DFT calculations performed with the Quantum Espresso package.[41,42] The Kohn−Sham equations are solved employing the Perdew−Burke−Ernzerhof (PBE) functional[43] to describe the exchange-correlation effects and ultrasoft pseudopotentials[44] to describe the electron−ion interaction. A plane-wave basis set with 38 Ry (380 Ry) cutoff was employed to represent the electronic wave functions (densities). Surface structures were represented by employing asymmetric $SnO_2(110)$ slabs composed of four atomic layers, and each layer corresponds to one SnO_2 unit. The atoms in the two bottom layers were kept fixed at their bulk positions. To prevent side interactions between periodic images, we employed a 2 × 2 surface supercell and a vacuum layer in the direction perpendicular to the surface of 15 Å. The Brillouin zone was sampled employing a 6 × 6 × 6 Monkhorst−Pack mesh[45] for the bulk calculations and reduced grids for surface calculations. All structures were relaxed by minimizing the atomic forces; the convergence threshold of energy and forces was set to 10^{-5} Ry and 10^{-4} Ry/Bohr, respectively. The final bulk-optimized lattice cell parameters are $a = b = 4.83$ Å and $c = 3.24$ Å. These values are in agreement with previously published experimental and theoretical data within 2% variations.[46]

To investigate the behavior of the proposed electrocatalyst, the Gibbs free energy profiles were calculated for the CO_2RR pathways to formic acid and carbon monoxide production at the surface. We compared the energy trends with the competing HER and catalyst self-reduction reaction, employing the computational hydrogen electrode (CHE) proposed by Nørskov and collaborators.[47] Free energy profiles display the free energy variation (ΔG) along the reduction reaction, from the reactants to the final products, through various intermediate states. The studied reactions involve the exchange of two electrons and two protons and a single intermediate step. From the analysis of the energy profiles, it is possible to determine the thermodynamic onset potential (U_{onset}) for each reaction defined as

$$U_{onset} = -\max \frac{[\Delta G^r(0\ \mathrm{V})\ ]}{n_e}$$

where ΔG^r is the free energy variation of a reaction step (r), while n_e represents the number of electrons exchanged in the step. For more details, see Supporting Information, Section 1.4.

https://doi.org/10.1021/acs.jpcc.2c02583
J. Phys. Chem. C 2022, 126, 14441−14447

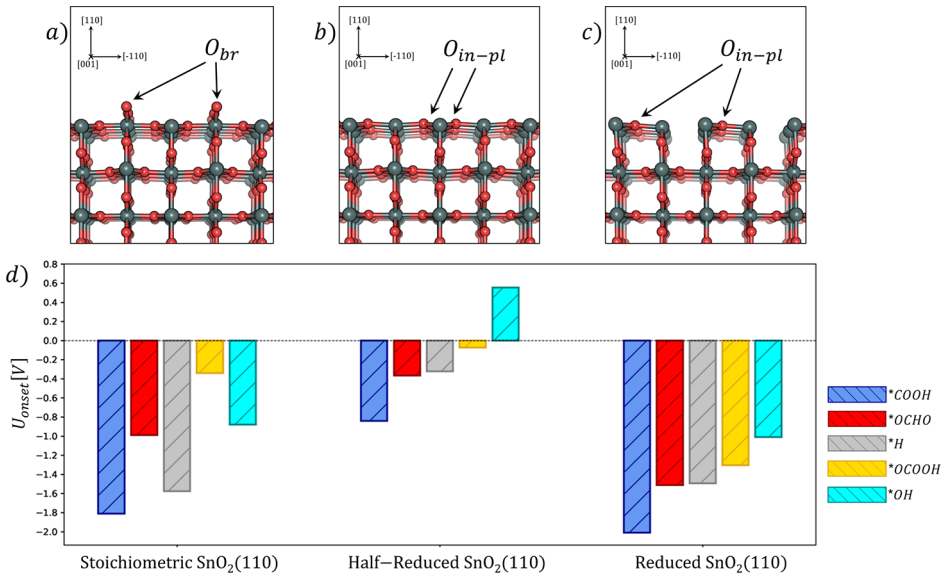

Figure 1. Side views of stoichiometric (a), half-reduced (b), and reduced (c) SnO_2(110) surface. Atom color code: Sn gray and O red. Panel d: U_{onset} vs RHE for CO_2RR, HER and self-reduction mechanisms on SnO_2(110) surfaces at increasing reduction degree. Reaction intermediate color code: *COOH blue, *OCHO red, *H gray, *OCOOH yellow, and *OH cyan.

Finally, because of the introduction of systematic errors in the calculation of the total energies of CO and CO_2 by PBE functionals, statistical corrections to OCO-molecules (reactants, intermediates, and products) were applied.[48] Solvation corrections were included as reported in the Supporting Information.

RESULTS AND DISCUSSION

To understand SnO_2 reactivity toward the CO_2RR, we focused our study on the low-index (110) facet, which is known to represent the thermodynamically most stable SnO_2 surface.[49] As detailed in the Introduction, experimental investigations have not succeeded in uniquely identifying the structure and stoichiometry of the tin oxide surface during CO_2 electroreduction. We thus calculated the free energy profiles of competing reduction reactions on the SnO_2(110) surface at different surface stoichiometries (i.e., reduction degree). In particular, for a given surface structure, we considered several competing processes that may take place at an oxide electrode surface under applied bias: noncatalytic surface self-reduction processes, CO_2RR and HER.

Self-reduction typically occurs at an oxide surface through reactions that involve the successive loss of surface oxygen species and the formation of understoichiometric structures. Both CO_2 and H^+ in the electrolyte may react with the surface oxygens (*O) by respectively forming carbonate and water as products, according to the following processes

$$CO_2 + 2(H^+ + e^-) + {}^*O \rightarrow H_2CO_3 + V_O \quad (1)$$

$$2(H^+ + e^-) + {}^*O \rightarrow H_2O + V_O \quad (2)$$

During these reactions, the proton-electron transfer generates surface oxygen vacancies (V_O), and correspondingly, Sn rich layers form. Reaction 1 unfolds into two steps

$$CO_2 + (H^+ + e^-) + {}^*O \rightarrow {}^*OCOOH \quad (1a)$$

$${}^*OCOOH + (H^+ + e^-) \rightarrow H_2CO_3 + V_O \quad (1b)$$

occurring via formation of a bicarbonate (*OCOOH) intermediate attached to the surface which is then released as carbonic acid. Reaction 2 is also split in two steps

$$(H^+ + e^-) + {}^*O \rightarrow {}^*OH \quad (2a)$$

$${}^*OH + (H^+ + e^-) \rightarrow H_2O + V_O \quad (2b)$$

and proceeds via formation of a surface hydroxyl (*OH) which is then released as water.

On the contrary, when the surface works as an electrocatalyst, CO_2 can be reduced either to formic acid or to carbon monoxide via two sequential proton-electron ($H^+ + e^-$) transfers

$$CO_2 + 2(H^+ + e^-) \rightarrow HCOOH \quad (3)$$

$$CO_2 + 2(H^+ + e^-) \rightarrow CO + H_2O \quad (4)$$

These two reduction reactions are competing and proceed as follows

$$CO_2 + (H^+ + e^-) \rightarrow {}^*OCHO \quad (3a)$$

$${}^*OCHO + (H^+ + e^-) \rightarrow HCOOH \quad (3b)$$

and

$$CO_2 + (H^+ + e^-) \rightarrow {}^*COOH \quad (4a)$$

$${}^*COOH + (H^+ + e^-) \rightarrow CO + H_2O \quad (4b)$$

Path (3) involves an *OCHO intermediate, formed after a first ($H^+ + e^-$) pair transfer. This intermediate then transforms into HCOOH upon reaction with a second ($H^+ + e^-$) pair. Path (4) proceeds instead through a *COOH intermediate that leads to the release of CO and water.[50]

In aqueous solution, the CO_2RR competes also with the HER according to the following reaction

$$2(H^+ + e^-) \rightarrow H_2 \quad (5)$$

which typically consists of the following two steps

https://doi.org/10.1021/acs.jpcc.2c02583
J. Phys. Chem. C 2022, 126, 14441−14447

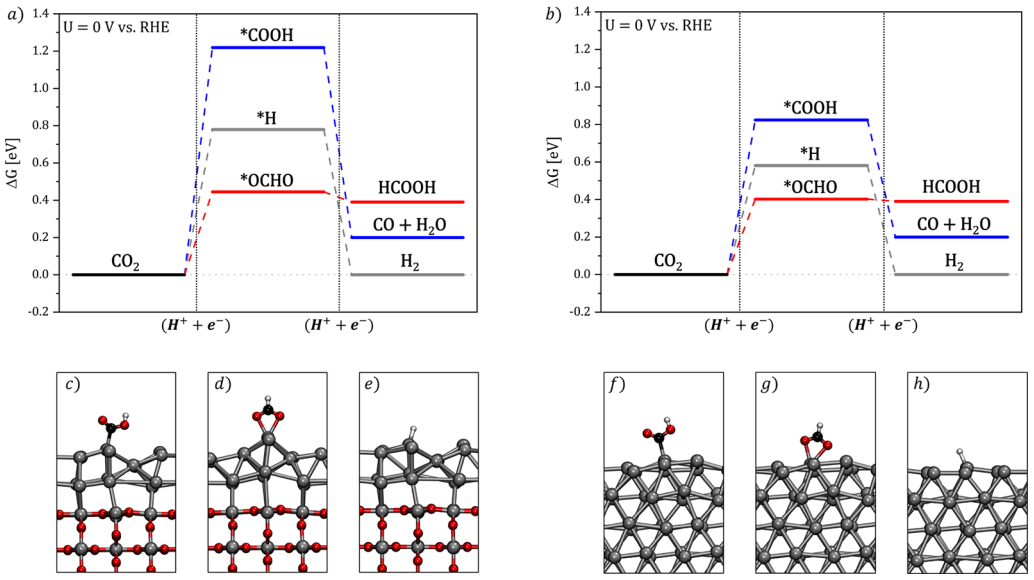

Figure 2. CO_2RR reaction paths to HCOOH and CO through *OCHO (red line) and *COOH (blue line) intermediates, respectively. HER reaction paths are also included (gray line). Panel a: 2Sn@SnO_2 surface at U = 0 V with respect to RHE and relative *COOH, *OCHO, and *H adsorbates (panels c, d, and e, respectively). Panel b: Sn(101) surface at U = 0 V with respect to RHE and relative *COOH, *OCHO and *H adsorbates (panels f, g and h, respectively). Atom color code: Sn gray, O red, H white, and C black.

$$(H^+ + e^-) \rightarrow {}^*H \tag{5a}$$

$${}^*H + (H^+ + e^-) \rightarrow H_2 \tag{5b}$$

involving the adsorption of atomic hydrogen (*H) at the surface.

To understand if the SnO_2(110) self-reduces or if it works as an electrocatalyst, we calculated the thermodynamics of the reaction paths of the reactions mentioned above and compared the values of the predicted onset potentials for surfaces at varying stoichiometry. U_{onset} determines the potential-limiting step of the overall reaction pathway and allows predicting which reaction preferentially occurs at a given applied bias. For a given surface structure, the reaction path characterized by the lowest U_{onset} is thermodynamically favored.

Figure 1d compares U_{onset} values obtained from the free energy profiles for CO_2RR, HER, and self-reduction on the SnO_2(110) surface for different surface stoichiometries. Free energy profiles for the CO_2RR, HER, and self-reduction reactions at the stoichiometric, half-reduced, and reduced SnO_2(110) surfaces are reported in Section 3 of the Supporting Information.

We start our analysis from the stoichiometric SnO_2(110) surface whose geometry is represented in Figure 1a. This surface exposes oxygen atoms in a so-called bridging configuration (O_{br}) and under-coordinated Sn ions. The potential-limiting steps for the CO_2RR and HER are the adsorption of carbon dioxide (reactions 3a and 4a) and the adsorption of hydrogen (5a) respectively, while for self-reduction, it is the removal of the final product (reactions 1b and 2b). On the stoichiometric surface, our calculations showed that the O_{br} atoms were the preferred species for binding CO_2 and H adsorbates, in the form of *OCOOH and *OH, respectively, with negative adsorption free energies. The relaxed geometries of carbonate and hydroxyl intermediates are reported in Figure S7 of the Supporting Information. The adsorption of *OCOOH species (Figure S7d) shows the lowest U_{onset} value (−0.34 V vs RHE), suggesting that, in the presence of dissolved CO_2, the self-reduction of the stoichiometric SnO_2(110) surface (Figure 1a) occurs via the carbonate intermediate. This indicates that the evolution of SnO_2(110) under applied bias initially leads to a complete loss of the oxygen bridging atoms, giving rise to a surface geometry which in the literature is indicated as half-reduced (Figure 1b).

The analysis of the competing reaction onset potentials on the half-reduced surfaces shows that at the potential required to remove O_{br}, self-reduction processes are still preferred. At this stage, protons spontaneously adsorb ($\Delta G^{2a} < 0$) on the exposed in-plane surface oxygens ($O_{in\text{-}pl}$) which are moved out of plane and generate hydroxyl species as represented in Figure S1b. These *OH are then released as H_2O molecules, leading to a further reduction of the SnO_2 surface to what in the literature is reported as reduced SnO_2(110) surface (Figure 1c). From an analysis of the graph reported in Figure 1d, it is apparent that further reduction of this surface structure occurs at higher external biases, though still lower than those required to reduce CO_2 to CO or HCOOH (U_{onset} − 2.00 and − 1.51 V vs RHE, respectively), or for HER (−1.49 V). Indeed, the remaining $O_{in\text{-}pl}$ atoms at −1.01 V vs RHE are further removed from the surface via proton adsorption and release of water molecules (Figure S7c). As a result, at relatively low potentials (about −1.01 V vs RHE) the preferred reaction occurring at the SnO_2(110) surface consists of the successive removal of oxygen atoms (first O_{br} and then $O_{in\text{-}pl}$) which ultimately leads to a surface exposing tin atoms only. In this potential range, the surface does not work as a catalyst, but it gets modified under the effect of the external bias, evolving toward Sn rich terminations. These results can be better understood by analyzing the projected density of states of different reaction intermediates at the SnO_2(110) surface at varying stoichiometry (Figure S11 in the Supporting Information): formation of *OH and *OCOOH species (intermediates leading to surface self-reduction) is more favored than *OCHO one (intermediate that leads to formic acid) as proven by the deeper energy of the corresponding bonding states. Until there are available oxygen atoms at the SnO_2(110) surface, *OH and

https://doi.org/10.1021/acs.jpcc.2c02583
J. Phys. Chem. C 2022, 126, 14441−14447

*OCOOH are preferred and the surface self-reduces. Given these results, we studied the catalytic activity of the system when an increasing number of metallic tin layers are formed at the oxide surface. In particular, we analyzed the $SnO_2(110)$ surface reactivity when one or two tin layers are exposed and compared the results to the surface of metallic tin.

When a single tin layer is formed at the top of the $SnO_2(110)$ facet (1Sn@SnO_2, Figure S8a), the surface appears to be still inactive toward both the CO_2RR and HER (Figure S8b). Indeed, at the first proton-electron transfer, all three-adsorption steps (reactions 3a, 4a, and 5a) have negative free energies. Moreover, the product formation (steps 3b, 4b, and 5b) corresponds to the potential-limiting step and the production of HCOOH involves the highest thermodynamic free energies (ΔG^{3b} = 1.04 eV) compared to CO (ΔG^{4b} = 0.52 eV) and H_2 (ΔG^{5b} = 0.53 eV).

When, instead, SnO_2 reduction proceeds to form a bilayer of tin on the surface (2Sn@SnO_2, Figure S10), the catalytic behavior completely changes, and the system becomes selective toward formic acid. This is evident from the analysis in Figure 2a (U_{onset} = −0.44 V vs RHE) in which, for comparison, we reported the free energy profile for the CO_2RR and HER (at U = 0 V vs RHE) both at the 2Sn@SnO_2 (panel a) and at a metal Sn(101) surface (panel b). The latter represents one of the most stable tin surfaces according to previous literature studies.[51] In the case of the CO_2RR, both reduction paths to HCOOH (red path) and CO (blue path) were considered.

Analyzing the two panels of Figure 2, we observe that the three competing reaction pathways show similar energy profiles, suggesting that processes are not spontaneous at U = 0 V vs RHE and require the application of a negative U_{onset}. The first proton-electron transfer is uphill, and it determines the U_{onset} of the reaction on both surfaces.

As for the CO_2RR, the formation of *COOH species is thermodynamically less favored with respect to *OCHO intermediates. Particularly, the energy needed to convert CO_2 to *COOH is markedly higher on the 2Sn@SnO_2 surface (ΔG^{4a} = 1.22 eV) if compared to Sn(101) (ΔG^{4a} = 0.82 eV). On the contrary, the free energy profile corresponding to *OCHO adsorbate on the tin bi-layered oxide is consistently similar (ΔG^{3a} = 0.44 eV) to the pristine metallic surface (ΔG^{3a} = 0.40 eV). This result demonstrates that these reduced surfaces are selective toward the production of formic acid.

With respect to the HER, Figure 2 highlights that the formation of *H intermediates is disfavored on the 2Sn@SnO_2 (ΔG^{5a} = 0.78 eV) if compared to Sn(101) (ΔG^{5a} = 0.58 eV). This confirms that the selectivity toward HCOOH is higher in partially reduced SnO_2 surfaces exposing at least two metallic tin layers. When the surface reduction proceeds giving rise to thick tin metallic phases, the hydrogen evolution reaction becomes possible and HCOOH faradaic efficiency is expected to decrease.

CONCLUSIONS

In conclusion, our results show that $SnO_2(110)$ surfaces are not intrinsically catalytically active for the CO_2RR or HER, but they reduce under an applied external bias, originating structures exposing tin atoms only. Moreover, our calculations show that as soon as a metallic tin bilayer is formed at the SnO_2 surface, the material selectively reduces CO_2 to formic acid. These findings are important to interpret experimental results and to identify the relevant CO_2RR catalytic active sites in SnO_2. In fact, several measurements, including operando, show that under working CO_2RR conditions both zerovalent tin and oxidized tin species are detected.[35,36] According to our results, a thin layer of Sn^0 is involved in the catalytic reaction, while the signal of oxidized tin species observed experimentally originates from subsurface layers which are not directly in contact with the electrolyte. Because two tin layers are enough to give selectivity toward formic acid, highlighting such structure may be very difficult with standard experimental techniques such as XRD. Moreover, when the catalyst is analyzed ex situ, the few reduced tin layers most probably quickly re-oxidize and their presence becomes undetectable. When a higher bias is applied, a thick layer of reduced tin layers is formed and, although the system is still catalytically active, our calculations show that the evolution of formic acid and hydrogen becomes thermodynamically competitive, and the catalyst loses in selectivity.

ASSOCIATED CONTENT

Supporting Information

The Supporting Information is available free of charge at https://pubs.acs.org/doi/10.1021/acs.jpcc.2c02583.

Gibbs free energy and reaction Gibbs free energy calculations, optimized structures, surface energy stability and projected density of states (PDF)

AUTHOR INFORMATION

Corresponding Authors

Clara Salvini − *Center for Sustainable Future Technologies, Istituto Italiano di Tecnologia, Turin 10144, Italy; Department of Applied Science and Technology, Politecnico di Torino, Turin 10129, Italy;* orcid.org/0000-0002-8451-7896; Phone: +39 011 090 7343; Email: clara.salvini@polito.it

Michele Re Fiorentin − *Center for Sustainable Future Technologies, Istituto Italiano di Tecnologia, Turin 10144, Italy;* orcid.org/0000-0002-1074-0411; Phone: +39 011 090 4333; Email: michele.refiorentin@iit.it

Authors

Francesca Risplendi − *Department of Applied Science and Technology, Politecnico di Torino, Turin 10129, Italy;* orcid.org/0000-0002-1277-6733

Federico Raffone − *Center for Sustainable Future Technologies, Istituto Italiano di Tecnologia, Turin 10144, Italy;* orcid.org/0000-0001-5045-7533

Giancarlo Cicero − *Department of Applied Science and Technology, Politecnico di Torino, Turin 10129, Italy;* orcid.org/0000-0002-2920-9882

Complete contact information is available at: https://pubs.acs.org/10.1021/acs.jpcc.2c02583

Author Contributions

The manuscript was written through contributions of all authors. All authors have given approval to the final version of the manuscript.

Notes

The authors declare no competing financial interest.

ACKNOWLEDGMENTS

The authors acknowledge CINECA for the availability of high-performance computing resources under the Iscra-C initiative

as well as the computational support provided by HPC@POLITO (http://www.hpc.polito.it).

REFERENCES

(1) Mac Dowell, N.; Fennell, P. S.; Shah, N.; Maitland, G. C. The role of CO_2 capture and utilization in mitigating climate change. *Nat. Clim. Change* **2017**, *7*, 243−249.

(2) Dibenedetto, A.; Angelini, A.; Stufano, P. Use of carbon dioxide as feedstock for chemicals and fuels: Homogeneous and heterogeneous catalysis. *J. Chem. Technol. Biotechnol.* **2014**, *89*, 334−353.

(3) Costentin, C.; Robert, M.; Savéant, J. M. Catalysis of the electrochemical reduction of carbon dioxide. *Chem. Soc. Rev.* **2013**, *42*, 2423−2436.

(4) Whipple, D. T.; Kenis, P. J. A. Prospects of CO_2 utilization via direct heterogeneous electrochemical reduction. *J. Phys. Chem. Lett.* **2010**, *1*, 3451−3458.

(5) Jouny, M.; Luc, W.; Jiao, F. General techno-economic analysis of CO_2 electrolysis systems. *Ind. Eng. Chem. Res.* **2018**, *57*, 2165−2177.

(6) She, Z. W.; Kibsgaard, J.; Dickens, C. F.; Chorkendorff, I.; Nørskov, J. K.; Jaramillo, T. F. Combining theory and experiment in electrocatalysis: Insights into materials design. *Science* **2017**, *355*, 1−12.

(7) Kumar, B.; Brian, J. P.; Atla, V.; Kumari, S.; Bertram, K. A.; White, R. T.; Spurgeon, J. M. New trends in the development of heterogeneous catalysts for electrochemical CO_2 reduction. *Catal. Today* **2016**, *270*, 19−30.

(8) Lee, H. J.; Kang, D. C.; Pyen, S. H.; Shin, M.; Suh, Y. W.; Han, H.; Shin, C. H. Production of H_2-free CO by decomposition of formic acid over ZrO_2 catalysts. *Appl. Catal., A* **2017**, *531*, 13−20.

(9) Wang, J.; Li, X.; Zheng, J.; Cao, J.; Hao, X.; Wang, Z.; Abudula, A.; Guan, G. Non-precious molybdenum-based catalyst derived from biomass: CO-free hydrogen production from formic acid at low temperature. *Energy Convers. Manage.* **2018**, *164*, 122−131.

(10) Grasemann, M.; Laurenczy, G. Formic acid as a hydrogen source - recent developments and future trends. *Energy Environ. Sci.* **2012**, *5*, 8171−8181.

(11) Schlapbach, L.; Züttel, A. Hydrogen-storage materials for mobile applications. *Nature* **2001**, *414*, 353−358.

(12) Yang, D.-R.; Liu, L.; Zhang, Q.; Shi, Y.; Zhou, Y.; Liu, C.; Wang, F.-B.; Xia, X.-H. Importance of Au nanostructures in CO_2 electrochemical reduction reaction. *Sci. Bull.* **2020**, *65*, 796−802.

(13) Lu, Q.; Rosen, J.; Zhou, Y.; Hutchings, G. S.; Kimmel, Y. C.; Chen, J. G.; Jiao, F. A selective and efficient electrocatalyst for carbon dioxide reduction. *Nat. Commun.* **2014**, *5*, 1−6.

(14) Jiang, B.; Zhang, X.-G.; Jiang, K.; Wu, D.-Y.; Cai, W.-B. Boosting formate production in electrocatalytic CO_2 reduction over wide potential window on Pd surfaces. *J. Am. Chem. Soc.* **2018**, *140*, 2880−2889.

(15) Gao, D.; Zhou, H.; Cai, F.; Wang, J.; Wang, G.; Bao, X. Pd-containing nanostructures for electrochemical CO_2 reduction reaction. *ACS Catal.* **2018**, *8*, 1510−1519.

(16) Back, S.; Yeom, M. S.; Jung, Y. Active sites of Au and Ag nanoparticle catalysts for CO_2 electroreduction to CO. *ACS Catal.* **2015**, *5*, 5089−5096.

(17) Detweiler, Z. M.; White, J. L.; Bernasek, S. L.; Bocarsly, A. B. Anodized indium metal electrodes for enhanced carbon dioxide reduction in aqueous electrolyte. *Langmuir* **2014**, *30*, 7593−7600.

(18) Liang, Y.; Zhou, W.; Shi, Y.; Liu, C.; Zhang, B. Unveiling in situ evolved In/In_2O_{3-x} heterostructure as the active phase of In_2O_3 toward efficient electroreduction of CO_2 to formate. *Sci. Bull.* **2020**, *65*, 1547−1554.

(19) Lee, C. W.; Hong, J. S.; Yang, K. D.; Jin, K.; Lee, J. H.; Ahn, H.-Y.; Seo, H.; Sung, N. E.; Nam, K. T. Selective electrochemical production of formate from carbon dioxide with bismuth-based catalysts in an aqueous electrolyte. *ACS Catal.* **2018**, *8*, 931−937.

(20) Jiang, H.; Wang, L.; Li, Y.; Gao, B.; Guo, Y.; Yan, C.; Zhuo, M.; Wang, H.; Zhao, S. High-selectivity electrochemical CO_2 reduction to formate at low overpotential over Bi catalyst with hexagonal sheet structure. *Appl. Surf. Sci.* **2021**, *541*, No. 148577.

(21) Blom, M. J. W.; Smulders, V.; van Swaaij, W. P. M.; Kersten, S. R. A.; Mul, G. Pulsed electrochemical synthesis of formate using Pb electrodes. *Appl. Catal., B* **2020**, *268*, No. 118420.

(22) He, Z.; Shen, J.; Ni, Z.; Tang, J.; Song, S.; Chen, J.; Zhao, L. Electrochemically created roughened lead plate for electrochemical reduction of aqueous CO_2. *Catal. Commun.* **2015**, *72*, 38−42.

(23) Zhao, S.; Li, S.; Guo, T.; Zhang, S.; Wang, J.; Wu, Y.; Chen, Y. Advances in Sn-based catalysts for electrochemical CO_2 reduction. *Nano-Micro Lett.* **2019**, *11*, 1.

(24) Li, Q.; Rao, X.; Sheng, J.; Xu, J.; Yi, J.; Liu, Y.; Zhang, J. Energy storage through CO_2 electroreduction: A brief review of advanced Sn-based electrocatalysts and electrodes. *J. CO2 Util.* **2018**, *27*, 48−59.

(25) Vasileff, A.; Xu, C.; Jiao, Y.; Zheng, Y.; Qiao, S.-Z. Surface and interface engineering in copper-based bimetallic materials for selective CO_2 electroreduction. *Chem* **2018**, *4*, 1809−1831.

(26) Feaster, J. T.; Shi, C.; Cave, E. R.; Hatsukade, T.; Abram, D. N.; Kuhl, K. P.; Hahn, C.; Nørskov, J. K.; Jaramillo, T. F. Understanding selectivity for the electrochemical reduction of carbon dioxide to formic acid and carbon monoxide on metal electrodes. *ACS Catal.* **2017**, *7*, 4822−4827.

(27) Bejtka, K.; Zeng, J.; Sacco, A.; Castellino, M.; Hernández, S.; Farkhondehfal, M. A.; Savino, U.; Ansaloni, S.; Pirri, C. F.; Chiodoni, A. Chainlike mesoporous SnO_2 as a well-performing catalyst for electrochemical CO_2 reduction. *ACS Appl. Energy Mater.* **2019**, *2*, 3081−3091.

(28) An, X.; Li, S.; Yoshida, A.; Wang, Z.; Hao, X.; Abudula, A.; Guan, G. Electrodeposition of tin-based electrocatalysts with different surface tin species distributions for electrochemical reduction of CO_2 to HCOOH. *ACS Sustainable Chem. Eng.* **2019**, *7*, 9360−9368.

(29) Del Castillo, A.; Alvarez-Guerra, M.; Solla-Gullón, J.; Sáez, A.; Montiel, V.; Irabien, A. Electrocatalytic reduction of CO_2 to formate using particulate Sn electrodes: Effect of metal loading and particle size. *Appl. Energy* **2015**, *157*, 165−173.

(30) Yadav, V. S. K.; Noh, Y.; Han, H.; Kim, W. B. Synthesis of Sn catalysts by solar electro-deposition method for electrochemical CO_2 reduction reaction to HCOOH. *Catal. Today* **2018**, *303*, 276−281.

(31) Pourbaix, M. *Atlas of Electrochemical Equilibria in Aqueous Solutions*, 2nd ed.; NACE International: Huston, 1974.

(32) Saravanan, K.; Basdogan, Y.; Dean, J.; Keith, J. A. Computational investigation of CO_2 electroreduction on tin oxide and predictions of Ti, V, Nb and Zr dopants for improved catalysis. *J. Mater. Chem. A* **2017**, *5*, 11756−11763.

(33) Lee, S.; Ocon, J. D.; Son, Y.; Lee, J. Alkaline CO_2 electrolysis toward selective and continuous $HCOO^-$ production over SnO_2 nanocatalysts. *J. Phys. Chem. C* **2015**, *119*, 4884−4890.

(34) Gao, T.; Kumar, A.; Shang, Z.; Duan, X.; Wang, H.; Wang, S.; Ji, S.; Yan, D.; Lu, L.; Liu, W.; et al. Promoting electrochemical conversion of CO_2 to formate with rich oxygen vacancies in nanoporous tin oxides. *Chin. Chem. Lett.* **2019**, *30*, 2274−2278.

(35) Dutta, A.; Kuzume, A.; Rahaman, M.; Vesztergom, S.; Broekmann, P. Monitoring the chemical state of catalysts for CO_2 electroreduction: an in operando study. *ACS Catal.* **2015**, *5*, 7498−7502.

(36) Kuzume, A.; Dutta, A.; Vesztergom, S.; Broekmann, P. Operando Raman spectroscopy: studies on the reactivity and stability of SnO_2 nanoparticles during electrochemical CO_2 reduction reaction. In *Encyclopedia of Interfacial Chemistry, Surface Science and Electrochemistry*; Wandelt, K., Ed.; Elsevier, 2018; pp 217−226.

(37) Li, L.; Zhao, Z.-J.; Hu, C.; Yang, P.; Yuan, X.; Wang, Y.; Zhang, L.; Moskaleva, L.; Gong, J. Tuning oxygen vacancies of oxides to promote electrocatalytic reduction of carbon dioxide. *ACS Energy Lett.* **2020**, *5*, 552−558.

(38) Cui, C.; Han, J.; Zhu, X.; Liu, X.; Wang, H.; Mei, D.; Ge, Q. Promotional effect of surface hydroxyls on electrochemical reduction of CO_2 over SnO_x/Sn electrode. *J. Catal.* **2016**, *343*, 257−265.

(39) Wei, Y.; Liu, J.; Cheng, F.; Chen, J. Mn-doped atomic SnO_2 layers for highly efficient CO_2 electrochemical reduction. *J. Mater. Chem. A* **2019**, *7*, 19651−19656.

https://doi.org/10.1021/acs.jpcc.2c02583
J. Phys. Chem. C 2022, 126, 14441−14447

(40) Zhang, Y.; Liu, J.; Wei, Z.; Liu, Q.; Wang, C.; Ma, J. Electrochemical CO_2 reduction over nitrogen-doped SnO_2 crystal surfaces. *J. Energy Chem.* **2019**, *33*, 22−30.
(41) Giannozzi, P.; Baroni, S.; Bonini, N.; Calandra, M.; Car, R.; Cavazzoni, C.; Ceresoli, D.; Chiarotti, G. L.; Cococcioni, M.; Dabo, I.; et al. QUANTUM ESPRESSO: A modular and open-source software project for quantum simulations of materials. *J. Phys.: Condens. Matter* **2009**, *21*, No. 395502.
(42) Giannozzi, P.; Andreussi, O.; Brumme, T.; Bunau, O.; Buongiorno Nardelli, M.; Calandra, M.; Car, R.; Cavazzoni, C.; Ceresoli, D.; Cococcioni, M.; et al. Advanced capabilities for materials modelling with Quantum ESPRESSO. *J. Phys.: Condens. Matter* **2017**, *29*, 465901.
(43) Perdew, J. P.; Burke, K.; Ernzerhof, M. Generalized gradient approximation made simple. *Phys. Rev. Lett.* **1996**, *77*, 3865−3868.
(44) Garrity, K. F.; Bennett, J. W.; Rabe, K. M.; Vanderbilt, D. Pseudopotentials for high-throughput DFT calculations. *Comput. Mater. Sci.* **2014**, *81*, 446−752.
(45) Monkhorst, H. J.; Pack, J. D. Special points for Brillouin-zone integrations. *Phys. Rev. B* **1976**, *13*, 5188.
(46) Sensato, F. R.; Custódio, R.; Calatayud, M.; Beltràn, A.; Andrés, J.; Sambrano, J. R.; Longo, E. Periodic study on the structural and electronic properties of bulk, oxidized and reduced SnO_2(1 1 0) surfaces and the interaction with O_2. *Surf. Sci.* **2002**, *511*, 408−420.
(47) Nørskov, J. K.; Rossmeisl, J.; Logadottir, A.; Lindqvist, L.; Kitchin, J. R.; Bligaard, T.; Jónsson, H. Origin of the overpotential for oxygen reduction at a fuel-cell cathode. *J. Phys. Chem. B* **2004**, *108*, 17886−17892.
(48) Risplendi, F.; Re Fiorentin, M.; Cicero, G. Unravelling electrocatalytic properties of metal porphyrin-like complexes hosted in graphene matrices. *2D Mater.* **2020**, *7*, No. 025017.
(49) Oviedo, J.; Gillan, M. J. The energetics and structure of oxygen vacancies on the SnO_2(110) surface. *Surf. Sci.* **2000**, *467*, 35−48.
(50) Kortlever, R.; Shen, J.; Schouten, K. J. P.; Calle-Vallejo, F.; Koper, M. T. M. Catalysts and reaction pathways for the electrochemical reduction of carbon dioxide. *J. Phys. Chem. Lett.* **2015**, *6*, 4073−4082.
(51) Hörmann, N. G.; Grossa, A.; Kaghazchi, P. Semiconductor-metal transition induced by nanoscale stabilization. *Phys. Chem. Chem. Phys.* **2015**, *17*, 5569−5573.

https://doi.org/10.1021/acs.jpcc.2c02583
J. Phys. Chem. C 2022, 126, 14441−14447